Tin dioxide nanoparticles as catalyst precursors for plasma-assisted vapor–liquid–solid growth of silicon nanowires with well-controlled density

Letian Dai, Isabelle Maurin, Martin Foldyna, José Alvarez, Weixi Wang, Hamza Mohsin, Wanghua Chen, Jean-Paul Kleider, Jean-Luc Maurice, Thierry Gacoin, et al.

Tin dioxide nanoparticles as catalyst precursors for plasma-assisted vapor-liquid-solid growth of silicon nanowires with well-controlled density

Tin dioxide nanoparticles as catalyst precursors for plasma-assisted vapor-liquid-solid growth of silicon nanowires with well-controlled density

Letian Dai[1,2,3], Isabelle Maurin[3,*], Martin Foldyna[2,*], José Alvarez[1,*], Weixi Wang[2], Hamza Mohsin[2,3], Wanghua Chen[2], Jean-Paul Kleider[1], Jean-Luc Maurice[2], Thierry Gacoin[3] and Pere Roca i Cabarrocas[2]

[1]GeePs, CNRS, CentraleSupelec, Université Paris-Sud, Université Paris-Saclay, Sorbonne Université-UPMC Université Paris 06, 91192 Gif-sur-Yvette Cedex, France

[2]LPICM, CNRS, Ecole Polytechnique, Université Paris-Saclay, 91128 Palaiseau, France

[3]Physique de la Matière Condensée, CNRS, Ecole Polytechnique, Université Paris-Saclay, 91128 Palaiseau, France

*E-mail : isabelle.maurin@polytechnique.edu;
martin.foldyna@polytechnique.edu;
jose.alvarez@geeps.centralesupelec.fr.

ABSTRACT: The fabrication of arrays of silicon nanowires (Si NWs) with well-defined surface coverage using the vapor-liquid-solid (VLS) process requires a good control of the density and size distribution for the metal catalyst. We report on a cost-effective bottom-up

approach to produce Si NWs by a low-temperature deposition technology using plasma-enhanced chemical vapor deposition (PECVD) and tin dioxide (SnO_2) nanoparticles as the source of tin catalyst. This strategy offers a straightforward method to select specific particle sizes by conventional colloidal techniques, and to tune the surface coverage using a polyelectrolyte layer to efficiently immobilize the particles on the substrate by electrostatic grafting. After a further step of reduction into tin metal droplets using hydrogen plasma treatment, the catalyst particles are used for the growth of Si NWs. This approach allows to produce controlled Si NWs arrays which can be used as a template for radial-junction thin film solar cells.

1. INTRODUCTION

Solar energy is one important renewable energy source for the future. Photovoltaic (PV) solar cells provide a seducing shortcut to directly convert sunlight into a very convenient form of energy which is electricity. In 2005, Kayes *et al.* fabricated radial junction (RJ) solar cells based on coaxial silicon nanowires (Si NWs) [1]. This new generation of cost-effective solar cells has been further improved and has already resulted in an efficiency of 9.2 % with a single p-i-n RJ (p-core Si NW) and 100 nm thick absorber layer [2]. The radial junction architecture benefits from strong light trapping and efficient carrier collection [3], leading to an increase in overall efficiency of the RJ solar cells. Optical modeling indicates that the density of Si NWs should be of the order of 10^8 NW/cm^2 for optimized performance [4]. Simulations have also shown that the n-i-p structure (with n-core Si NW) should give higher power conversion efficiency (as high as 12 %) [5] than the p-i-n configuration. Moreover, tandem structures result in a larger absorption spectrum and higher open circuit voltage (V_{oc}) that have a potential for improving further the performance of RJ solar cells [6]. At the present stage, optical design is mainly based on the control of the density, size distribution, and morphology of the Si NWs forest. In addition, the PV functionality relies strongly on the uniformity and quality of intrinsic and doped layers around the Si NW cores, which enforces a sufficient space between NWs for the subsequent formation of radial junctions.

Vapor-liquid-solid (VLS) growth is a bottom-up technique for the fabrication of Si NWs [7]. This process involves the use of a metal catalyst that acts as a seed for the growth of NWs, which is usually achieved by chemical vapor deposition (CVD), but it can also be carried out by plasma-enhanced CVD (PECVD) at lower temperatures. Gold [8], aluminum [9], bismuth [10], indium [11], and tin [11,12] have been employed as catalysts for the growth of Si NWs in the past. Sn is a good candidate because of its low melting temperature (231.9 °C), low cost, abundance, and ability to prevent the formation of deep defect levels in the silicon lattice. Moreover, it was recently shown that it is possible to catalyze Si NWs in the metastable hexagonal-diamond structure [13], the calculated band structure of which presents several interesting features, including a direct band gap in thin NWs [14].

First attempts to grow Si NWs through the surface reduction of SnO_2 or ITO coatings by H_2 plasma treatment have already been reported [12]. Better defined catalyst distributions were achieved using thermal evaporation of Sn in high vacuum, which led to the formation of a thin film of Sn on the substrate [12,15,16]. Upon dewetting, this evaporated Sn layer forms isolated droplets. In order to have forests of Si NWs with uniform diameter and length, a narrow size distribution of the tin catalyst is necessary, with mean particle sizes around 50 nm. As already mentioned, the final NW density has a large impact on light absorption and therefore on the short circuit current of radial junction solar cells, so that a well-defined density of Sn droplets is also required to optimize NW based devices. The standard approach for controlling the Si NWs density is to control the density of catalyst particles by varying the thickness of the thermally evaporated tin film [12,15,16]. However, it is not easy to independently tune the size of the Sn droplets and their density by the thermal evaporation of Sn or surface reduction of SnO_2 coatings [17]. For instance, large spacing between Sn droplets of around 1 µm with 10 to 100 nm particle sizes cannot be achieved. An efficient alternative is to use electron beam lithography to obtain well-defined catalyst size and specific localization, but such process is obviously expensive and hardly scalable.

The present work investigates an alternative method for the control of the catalyst distribution using colloidal solutions of SnO_2 nanoparticles (NPs) deposited onto the surface by wet-chemical routes. In particular, we aim at NPs' density smaller than 10^8 cm^{-2}, which cannot be obtained with evaporated Sn for future tandem architecture. Solutions of SnO_2 NPs can be obtained by direct synthesis using conventional colloidal chemistry [18,19]. Herein, we focus on a very simple and scalable approach based on the dispersion of particles extracted from commercially available SnO_2 nanocrystalline powders. The main challenges are related to the size selection (targeted to be around 50 nm with low size polydispersity) and appropriate dispersion of particles extracted from the initial powder to form colloids that are stable over time. Starting from these colloidal suspensions, different methods can be used for their deposition on a substrate such as spin or dip-coating, but electrostatic grafting was preferred considering the ability to have uniform distributions on the surface and a simple

control of the particles density [20,21]. At first, a monolayer of a charged polymer is deposited on the substrate, with an electric charge opposite to that of the SnO_2 NPs. In a second step, the substrate is immersed for a given duration in the colloidal solution, and then rinsed extensively to remove non-grafted particles. With the assistance of the hydrogen plasma, the reduction of SnO_2 into Sn can be realized at a relatively low temperature (~ 250 °C) as compared to thermal treatment in a hydrogen atmosphere for which the onset of reduction is above 490 °C [22]. In this work, we studied plasma-assisted reduction from SnO_2 to metallic Sn and its impact on the final distribution of the Sn catalyst. Then, the density of Si NWs was eventually investigated in relation to the Sn droplets with controlled distribution.

2. EXPERIMENTAL SECTION

Tin dioxide NP powder with a purity of 99.5 % and 55 nm nominal particle size was purchased from Goodfellow. The as-received powder mostly contains micrometer-sized aggregates and requires a preliminary step of ball milling before dispersion in alkaline aqueous solution. The tin dioxide powder (4.5 g) was mixed with 14 mL diethylene glycol (DEG, ≥99.0 %, Sigma-Aldrich) and placed with 150 zirconia balls of 5 mm-diameter in a 40 mL ZrO_2 bowl. This mixture was ball-milled using a FRITSCH Pulverisette 6 for 10 cycles of 15 min at 600 rpm with a rest time of 6 min between each cycle to minimize heating. The concentrated suspension was then dropwise added into a solution of tetramethylammonium hydroxide (TMAOH) obtained from a 25 wt% TMAOH solution (Sigma-Aldrich) after dilution with ultrapure water to tune the pH value from 9 to 13. A volume of 1 mL of SnO_2/DEG mixture diluted in 99 mL of TMAOH solution corresponds to a concentration of about 3.2 g/L. Particle size selection was achieved by differential centrifugation (Fisher Bioblock Scientific Sigma 3K10) with accelerations ranging from 1,000 to 11,000 g (gravity) for 5 min. After elimination of the precipitate, nanoparticles were recovered from the supernatant. Their immobilization was achieved onto silicon wafers after a preliminary cleaning. This step consists of immersing the substrate in 3 % TFD4 solution in water for 20 min followed by extensive rinsing with water, drying using a N_2

gas stream and UV/ozone treatment at 50 °C for 15 min to remove residual organic contaminations. Poly(diallyldimethylammonium) chloride (PDDAc, molecular weight 100,000 - 200,000) was purchased from Aldrich (20 wt% solution of PDDAc in water). The cleaned silicon wafers were immersed in a diluted 0.2 wt% PDDAc aqueous solution for 10 min, then thoroughly rinsed with deionized water and blown dried under a stream of nitrogen. The Si wafer surface was thus functionalized by a $PDDA^+$, Cl^- monolayer. 1 mL of SnO_2 colloidal suspension was then deposited on the substrate and left for 5 min, then rinsed with deionized water and dried by nitrogen gas flow. The resulting samples were heated up to 450 °C in the air for 1.5 hours (with 5 °C/min ramping) to remove the PDDA overlay.

Two different procedures were carried out to reduce SnO_2 to metallic Sn: (i) hydrogen plasma treatment in a plasma reactor using a flow rate of 100 sccm (standard cubic centimeters per minute) H_2 under 0.8 mbar pressure at 400 °C for 10 min and a RF power of 10 Watt; or (ii) thermal treatment under reductive atmosphere (10% H_2 and 90 % Ar) at 700 °C at a pressure of 1 bar for 30 min. After these reduction steps, the samples were taken out into the air. Some reduced Sn droplets were recovered for analysis by transmission electron microscopy (TEM). These particles were transferred to a TEM grid by scratching with a tweezer and immersing in a little amount of isopropanol.

The Si NWs were grown on plasma-treated substrates previously characterized by scanning electron microscopy (SEM). Because of oxidation in air, growth involved several steps: H_2 plasma treatment at 400 °C for 2 min, RF power of 10 Watt, followed by stopping the plasma, introducing 1 sccm silane (SiH_4) at the same temperature, waiting around 5 min and starting again the plasma with a RF power of 2 Watt for 60 min. The corresponding deposition rate of a-Si:H on reference Corning glass is 9.3 Å/min. Some Si NWs were transferred to TEM grids using the procedure described above for the tin particles.

Size, zeta potential, and dispersion state of the colloids, were characterized by Dynamic Light Scattering (DLS) using a Malvern Nano ZS zetasizer. A PANalytical X-Pert diffractometer equipped with Cu Kα radiation was used to characterize the commercial SnO_2 powder. Microstructural

characterizations were carried out by SEM and TEM. We used a Hitachi S4800 FEG-SEM operating at 10 kV. Size distribution, surface density and nearest neighbor distances of SnO_2 NPs were determined by analysis of the SEM images using the ImageJ software [23]. Statistics were carried out over more than 1000 particles. TEM imaging was carried out with a FEI Titan G2 ETEM (NanoMAX) operating at 300 kV and equipped with an objective lens Cs corrector, a High Angle Annular Dark Field (HAADF) Scanning Transmission Electron Microscopy (STEM) module and an energy-dispersive X-ray spectroscopy (EDS) detector.

3. RESULTS AND DISCUSSION

Preparation of SnO_2 dispersions and deposition onto silicon substrates. The commercial SnO_2 cassiterite nanopowder consists of tens of micrometer aggregates made of 55 nm primary nanoparticles (see Figure S1 in supplementary information). The powder was first dispersed in DEG and disaggregated by ball milling [24]. DEG was chosen because this solvent is polar and helps the dispersion by interacting with the surface of the NPs. Aliquots of this grounded suspension were then added to a TMAOH aqueous solution in order to ensure electrostatic repulsions between particles, as the point of zero charge (PZC) of SnO_2 cassiterite is 3.5-4.5 [25,26]. A colloidal solution with a particle concentration of ~3.2 g/L was prepared, starting from the 320 g/L grounded powder in DEG (hereafter named as 100-time diluted solution). Figure 1(a) shows the zeta potential of SnO_2 NPs in TMAOH solutions of pH values ranging between 9 and 13, after a preliminary centrifugation at 3,500 g to remove residual aggregates. The negative sign of the zeta potential indicates negatively charged SnO_2 particles. Usually, an absolute value over 30 mV is considered as a good indication of colloidal stability. For the 100-time diluted solution, we thus selected a pH of 12 as it yields the highest zeta potential absolute value. Such a suspension is stable over a week.

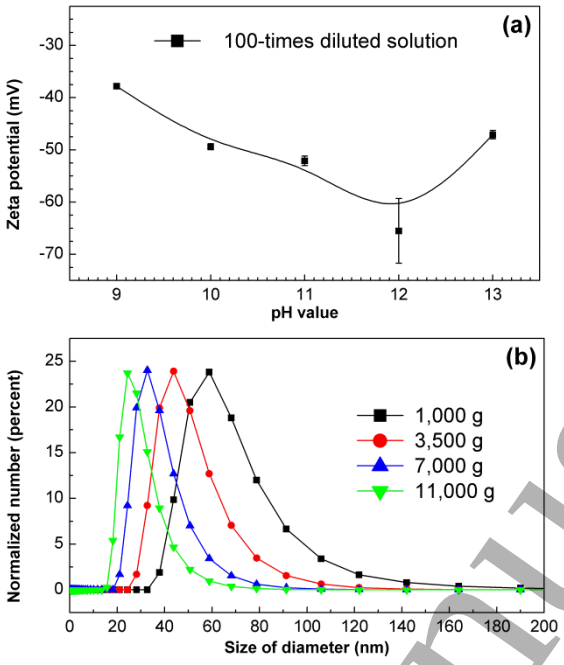

Figure 1. (a) Zeta potential of SnO_2 NPs after dilution (1/100 v/v) in TMAOH solutions of different pH values and centrifugation at 3,500 g for 5 min; The solid line is a guide to the eye (b) Size distribution of SnO_2 NPs in the supernatant for pH 12 TMAOH solutions after centrifugation at 1,000, 3,500, 7,000 and 11,000 g for 5 min.

The next step is a centrifugation to select individual particles and decrease the width of the size distribution. Indeed, high acceleration makes sedimentation of particles much faster with a size-dependent rate, so that big particles are recovered as a precipitate and the smallest ones remain in the supernatant. The diameter of these latter particles is directly dependent on the centrifugation speed as illustrated in Figure 1(b). This plot shows the size distribution of SnO_2 NPs in the supernatant after 5 min centrifugation at accelerations of 1,000, 3,500, 7,000 and 11,000 g, with a wider distribution and larger mean size observed for the solution centrifuged at 1,000 g as compared to the other cases.

At this stage, the SnO_2 NPs were deposited on silicon substrates. First, a thin layer of PDDAc was adsorbed onto the surface to graft the SnO_2 NPs and avoid their aggregation upon evaporation of the solvent. Then, this functionalized surface was immersed in the colloidal solution of size selected SnO_2 particles. The SEM images of Figures 2(a) to 2(d) are representative of the surface coverage after 5 min immersion using the SnO_2 suspensions of Figure 1(b), i.e. centrifuged at increasing acceleration. Statistical analyses of the particle sizes are in fair agreement with the DLS results: both the mean

value and the width of the size distribution decrease with the increase of the centrifugation speed, as shown in Figure 2(e). However, the mean particle size is systematically smaller than the one determined by DLS in the colloidal solution, as clearly observed after centrifugation at 1,000 g. To some extent, this could account for a higher adsorption rate of small particles (diameter around 30 nm) with respect to big ones. The area density of SnO_2 nanoparticles also decreases from 1.3×10^{9} NP/cm^{-2} to 1.4×10^{8} NP/cm^{-2} by increasing the centrifugation speed from 1,000 to 11,000 g. It results in an increase of the mean value of nearest neighbor distances, which are equal to ~150, 200, 270 and 420 nm in Figures 2(a) to 2(d), respectively. These SEM images also show that at 1,000 g and to a lesser extent at 3,500 g, some particles are still in the form of aggregates while at higher centrifugation speed they can be considered as individual ones.

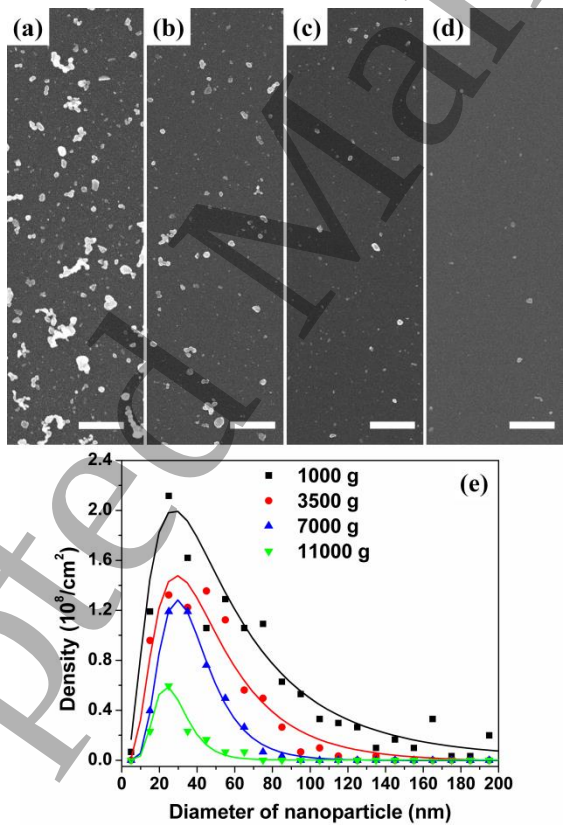

Figure 2. (a to d) SEM images representative of the distribution of SnO_2 NPs after 5 min immersion of the Si/PDDAc substrate in colloidal solutions centrifuged at: (a) 1,000, (b) 3,500, (c) 7,000 and (d) 11,000 g. Scale bar 500 nm. (e) Size distribution determined from selected SEM images with 10 nm bin size. Solid lines correspond to fits by lognormal functions.

The surface coverage decreases with the increase of the centrifugation speed, reflecting a decreased concentration of SnO_2 NPs in the TMAOH solutions. Indeed, if we compare the NP density for 100-time dilution (~ 3.2 g/L solution) vs. 1000-time dilution (~ 0.3 g/L) of the original DEG/SnO_2 mixture, we find a similar decrease of the surface coverage. Figures 3(a), 3(b) and 3(c) compare qualitatively and quantitatively the as-obtained densities for colloidal solutions that were both first centrifuged at 3,500 g for 5 min. This density of SnO_2 NPs is almost four times smaller in the case of the 1000-time dilution, with a mean nearest neighbor distance that increases from 200 nm to 370 nm with respect to the 100-time diluted solution. Moreover, the size distributions are nearly the same for the two dilutions. It means that the size polydispersity is mainly dependent on the acceleration of centrifugation. However, it is worth mentioning that the dilution should be performed before the size selective centrifugation steps. Otherwise, we found rather surprisingly that particles on the substrate are much more aggregated, whereas the distributions in the solution are comparable from DLS data. The reason for this difference remains unclear yet.

The present colloidal approach to control the density and the size of the catalyst NPs appears more accurate than thermal evaporation because those two quantities can be tuned independently. Moreover, low densities of SnO_2 NPs can be obtained in a straightforward and repeatable way.

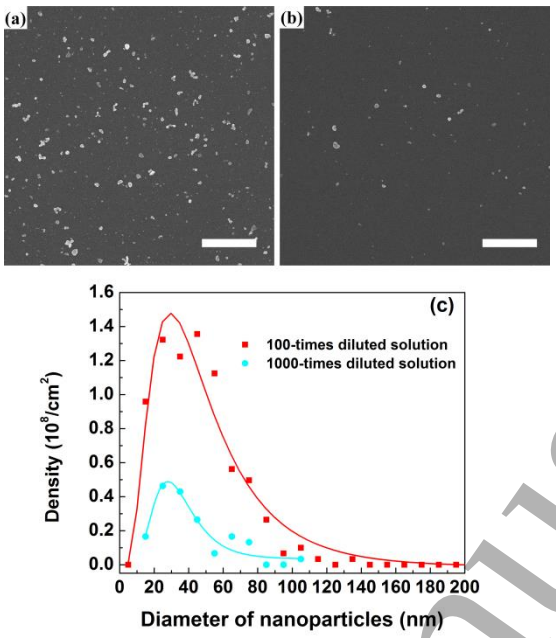

Figure 3. SEM images of SnO_2 NPs grafted onto functionalized Si/PDDAc surfaces using 1/100 v/v (a) and 1/1000 v/v (b) diluted solutions of the initial DEG/SnO_2 NP mixture and the same immersion time of 5 min. A preliminary centrifugation at 3,500 g for 5 min was performed before grafting. Scale bars: 1 µm in (a) and (b). (c) Size distribution of the SnO_2 NPs for dilutions (a) and (b), with 20 nm bin size. Solid lines are fits by lognormal functions.

Hydrogen reduction of SnO_2 NPs. We compared two reduction paths to turn the SnO_2 particles into metallic Sn: hydrogen plasma treatment and thermal reduction under H_2/Ar atmosphere. Figures 4 and S2 in the ESI show the effect of the above-mentioned treatments on SnO_2 NPs characterized by SEM. In the case of the hydrogen plasma treatment at 400 °C, the morphology of the NPs is strongly modified from slightly faceted to spherical likely because of a partial or complete transformation in a melt state (Sn: T_m = 231.9 °C). In addition, for well separated particles such as those targeted in the present work, this treatment does not lead to significant tin diffusion or droplet coalescence. Indeed, the comparison of Figures 4(c) and 4(d) or 4(e) and 4(f) shows similar distribution and localization of the catalyst particles before and after the plasma treatment. We do not expect a substantial change in the particle size upon reduction, except when coalescence occurs, because of the similar density of SnO_2 cassiterite and β-Sn (~7.0 and 7.3 g/cm^3, respectively). On the other hand, the thermal treatment

at 700 °C under H_2/Ar atmosphere did not modify the morphology of the catalyst particles. It only led to the formation of tiny dots of diameters of less than 5 nm at the particle surface, see Figures S2(a) and S2(b) in supplementary information.

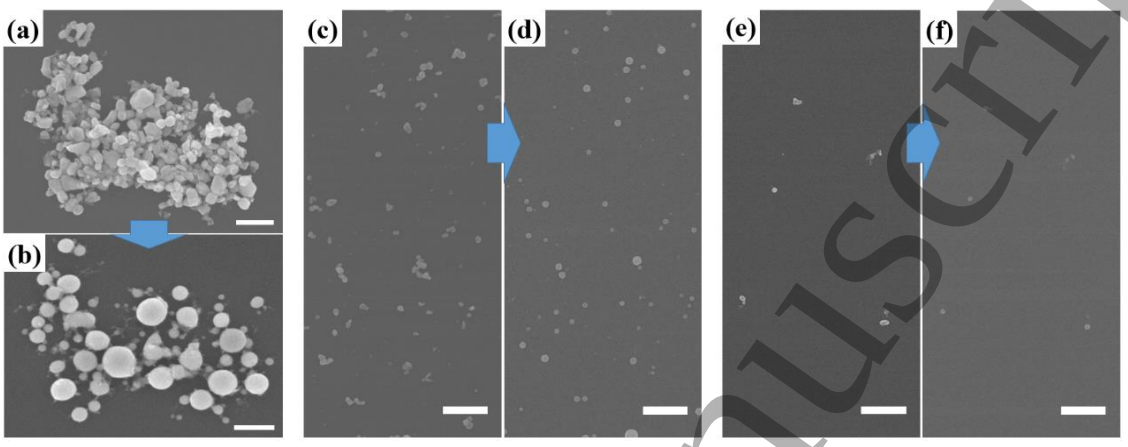

Figure 4. Top view SEM image of the same aggregate of SnO_2 particles (a) before and (b) after hydrogen plasma treatment at 400 °C. SnO_2 NPs deposited from the 100-time diluted solution after centrifugation at 3,500 g for 5 min with a rather large density (~ 9×10^8 NP/cm^2) (c) before and (d) after plasma reduction. SnO_2 NPs with lower density (~ 8×10^7 NP/cm^2) obtained from the 1000-time diluted solution after centrifugation at 11,000 g for 5 min (e) before and (f) after plasma reduction. Scale bars: 200 nm (a-b), 500 nm (c-f), respectively.

To study this reduction step more quantitatively, we have performed chemical mapping by STEM-EDS on catalyst particles transferred on a TEM grid after the H_2 plasma treatment and one month storage in ambient air. The comparison is made with pristine SnO_2 particles. Figure 5 summarizes the results of EDS elemental analysis. Figure 5(b) shows the intensity of oxygen K_α and tin L_α peaks, corresponding to the SnO_2 NP shown in Figure 5(a). The oxygen is present at the same concentration everywhere in the particle. Figure 5(d) shows the intensity of oxygen K_α and tin L_α peaks in two selected parts of the H_2 plasma-treated NP shown in Figure 5(c): the peak intensity ratio corresponds to the SnO_2 reference at the NP surface, but there is a much smaller oxygen signal in the center. Figure 5(e) shows the chemical map corresponding to the high-angle annular dark field (HAADF) image of Figure 5(c) and 5(f) displays the quantitative concentrations deduced from the two spectra in Figure

5(d). It is clear that the oxygen is mostly concentrated in the shell part. The atomic ratio between Sn and O is ~8:1 at the central part and ~1:1.8 in the shell part. The oxygen fraction of 11% in the central zone is mostly because we are also probing part of the outer shell. These data indicate that the central region of the SnO_2 NPs has been fully reduced by hydrogen plasma treatment but that the outside shell was re-oxidized after exposition to the air. As reported by other authors, hydrogen plasma reduction is thus much more efficient than the thermal reduction in hydrogen [22,27,28]. Moreover, the growth of Si NWs can be achieved in the same chamber just after plasma treatment, allowing for a single pump-down process.

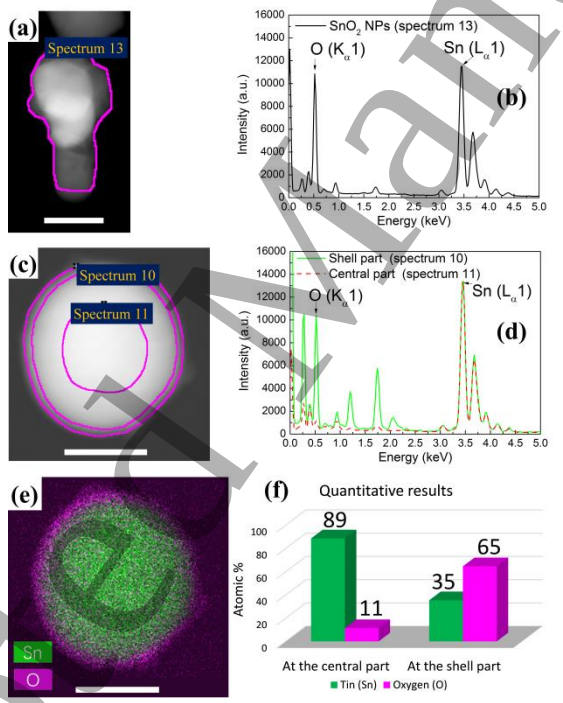

Figure 5. (a) STEM-HAADF image of a SnO_2 NP; (b) EDS spectrum corresponding to the region surrounded by the purple line in (a); (c) STEM-HAADF image of H_2-plasma reduced NP after storage in air for one month; (d) EDS spectrum (green solid line) recorded in the shell part of the particle shown in (c) and spectrum (red dashed line) recorded in the central part; (e) Element mapping of Sn (green) and O (pink) in STEM image (c); (f) Chart of quantitative results for Sn (green) and O (pink) in the central and shell parts. Scale bars in (a), (c) and (e) correspond to 50 nm.

Growth of Si NWs from the reduced metallic Sn droplets. After hydrogen plasma treatment, the distribution of metallic Sn droplets was characterized by SEM. Then, the samples were loaded in the plasma chamber again for NW growth as described in the experimental part. Note that separate reducing and growth steps are not necessary, and can be performed in a single pump-down. Here SEM observations were performed in between in order to precisely quantify the number of Si NWs formed per Sn catalyst drops. The Si NWs obtained by plasma-assisted VLS growth from the catalysts particles of Figures 4(d) and 4(f) are shown in Figures 6(a) and 6(b), respectively. Because the growth yield (the number of Si NWs divided by the number of catalyst nanoparticles) is generally small [29], the number of Si NWs formed is much lower than the density of Sn droplets. Nevertheless, the comparison of Figures 6(a) and 6(b) indicates that the final number of Si NWs is proportional to the initial density of catalysts. The ratio of number of NWs to the number of initial SnO_2 NPs is about 2:100.

In previous studies using evaporated Sn, the NW density could be controlled between 2×10^8 - 6×10^8 NW/cm^2 [17]. We have prepared many samples with reduced density using the present approach. For instance, the densities of Si NWs are ~ 2×10^6 NW/cm^2 and ~ 2×10^7 NW/cm^2 in the two cases shown in Figure 6(a) and 6(b). The use of colloidal solutions of catalyst particles that can be diluted on-demand can thus easily expand the range of Si NWs density down to less than 10^6 NW/cm^2.

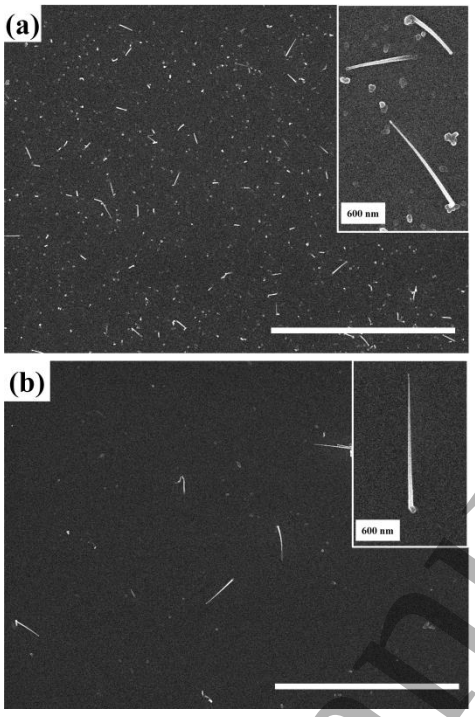

Figure 6. Top view SEM image of Si NWs grown by VLS using reduced Sn droplets acting as catalysts. Si NWs with density (a) ~ 2×10^7 NW/cm^2 and (b) ~ 2×10^6 NW/cm^2. Scale bar 10 μm.

Some Si NWs from the sample in Figure 6(a) were transferred to a TEM grid. Figure 7 shows a microstructure for a single NW, with a Sn droplet at the tip and a crystalline structure all along the wire. Fast Fourier Transform (FFT) analyses of selected regions are displayed in Figures 8(b), 9(b) and 9(c). They show that the core of the NW is a single crystal, most probably twinned (the pattern is not a standard diamond-cubic silicon pattern). However, there is a clear difference between the FFT patterns in Figure 9(b) and 9(c) taken at spots B-1 and B-2 at the bottom of the NW, which represent the core and shell regions respectively. The core is crystalline while the shell, at that level, is amorphous.

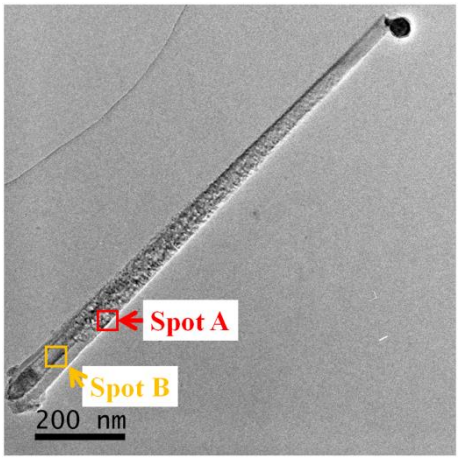

Figure 7. TEM image of one Si NW with a Sn droplet at the tip with two selected regions spot A and spot B.

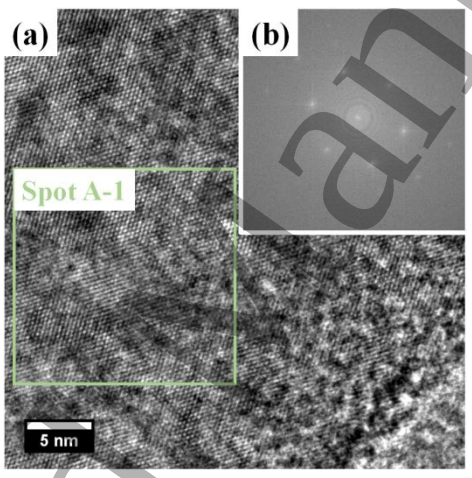

Figure 8. (a) HR-TEM image from spot A (red square) in Figure 7. (b) Fast Fourier Transform of the region into spot A-1 (green square) in (a).

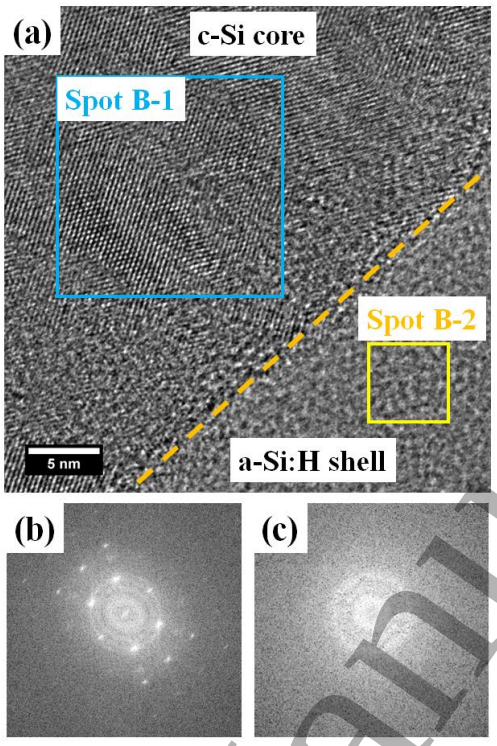

Figure 9. (a) HR-TEM image from spot B (orange square) in Figure 7. Fast Fourier Transform images (b) and (c) of the regions into the spots B-1 (blue square) and B-2 (yellow square) in (a), respectively.

4. CONCLUSIONS

This work has shown the potential and versatility of using SnO_2 nanoparticles as the source of tin catalyst for the growth of Si NWs. This method allows tuning the density of the catalyst droplets from 10^9 cm^{-2} down to at least 10^7 cm^{-2} in a reliable and reproducible way. The SnO_2 nanoparticles were fully reduced to metallic tin droplets at 400 °C in a H_2 plasma treatment. This allows performing both SnO_2 reduction and Si NW growth by plasma-assisted VLS in a single pump down process. We have successfully grown crystalline Si NWs using Sn reduced from SnO_2 NPs and verified its crystalline structure by TEM. Finally by combining this new approach of using SnO_2 NPs as precursor catalysts and previous results based on Sn thermal evaporation, it is possible to control the density of Si NWs within three orders of magnitudes, from 10^9 down to 10^6 cm^{-2}. Decreasing the density of grown NWs is necessary for the future development of tandem radial junction devices which involve a larger number of layers, leading to significantly larger diameters.

ACKNOWLEDGMENT

This work was financially supported by the project "SOLARIUM" ANR-14-CE05-0025 of the French National Research Agency (ANR). All TEM measurements were performed within the NanoMAX initiative, supported by the project "TEMPOS" ANR-12-BSV1-0029 of the French National Research Agency (ANR). The authors acknowledge H. Arezki for his preliminary work on the stabilization of SnO_2 NPs dispersions.

REFERENCES

[1] Kayes B M, Atwater H A and Lewis N S 2005 Comparison of the device physics principles of planar and radial p-n junction nanorod solar cells *J. Appl. Phys.* **97** 114302

[2] Misra S, Yu L, Foldyna M and Roca i Cabarrocas P 2015 New Approaches to Improve the Performance of Thin-Film Radial Junction Solar Cells Built Over Silicon Nanowire Arrays *IEEE J. Photovoltaics* **5** 40–5

[3] Wang C, Yu S, Chen W and Sun C 2013 Highly Efficient Light-Trapping Structure Design Inspired By Natural Evolution *Sci. Rep.* **3** 1025

[4] Foldyna M, Togonal A S, Rusli and Roca i Cabarrocas P 2017 Optimization and optical characterization of vertical nanowire arrays for core-shell structure solar cells *Sol. Energy Mater. Sol. Cells* **159** 640–8

[5] Diouf D, Ngo I, Kleider J-P, Gueunier-Farret M and Alvarez J 2012 Nanowire solar cells using hydrogenated amorphous silicon: A modeling study *Phys. status solidi* **209** 1026–30

[6] Qian S, Misra S, Lu J, Yu Z, Yu L, Xu J, Wang J, Xu L, Shi Y, Chen K and Roca i Cabarrocas P 2015 Full potential of radial junction Si thin film solar cells with advanced junction materials and design *Appl. Phys. Lett.* **107** 43902

[7] Wagner R S and Ellis W C 1964 VAPOR - LIQUID - SOLID MECHANISM OF SINGLE CRYSTAL GROWTH *Appl. Phys. Lett.* **4** 89 – 90

[8] Gudiksen M S and Lieber C M 2000 Diameter-Selective Synthesis of Semiconductor

Nanowires *J. Am. Chem. Soc.* **122** 8801–2

[9] Wang Y, Schmidt V, Senz S and Gösele U 2006 Epitaxial growth of silicon nanowires using an aluminium catalyst *Nat. Nanotechnol.* **1** 186–9

[10] Yu L, Fortuna F, O'Donnell B, Jeon T, Foldyna M, Picardi G and Roca i Cabarrocas P 2012 Bismuth-Catalyzed and Doped Silicon Nanowires for One-Pump-Down Fabrication of Radial Junction Solar Cells *Nano Lett.* **12** 4153–8

[11] Yu L, O'Donnell B, Alet P-J, Conesa-Boj S, Peiró F, Arbiol J and Roca i Cabarrocas P 2009 Plasma-enhanced low temperature growth of silicon nanowires and hierarchical structures by using tin and indium catalysts *Nanotechnology* **20** 225604

[12] Yu L, Alet P-J, Picardi G, Maurin I and Roca i Cabarrocas P 2008 Synthesis, morphology and compositional evolution of silicon nanowires directly grown on SnO_2 substrates *Nanotechnology* **19** 485605

[13] Tang J, Maurice J-L, Fossard F, Florea I, Chen W, Johnson E V., Foldyna M, Yu L and Roca i Cabarrocas P 2017 Natural occurrence of the diamond hexagonal structure in silicon nanowires grown by a plasma-assisted vapour–liquid–solid method *Nanoscale* **9** 8113–8

[14] Amato M, Kaewmaraya T, Zobelli A, Palummo M and Rurali R 2016 Crystal Phase Effects in Si Nanowire Polytypes and Their Homojunctions *Nano Lett.* **16** 5694–700

[15] Alet P-J, Yu L, Patriarche G, Palacin S and Roca i Cabarrocas P 2008 In situ generation of indium catalysts to grow crystalline silicon nanowires at low temperature on ITO *J. Mater. Chem.* **18** 5187

[16] Yu L, O'Donnell B, Foldyna M and Roca i Cabarrocas P 2012 Radial junction amorphous silicon solar cells on PECVD-grown silicon nanowires *Nanotechnology* **23** 194011

[17] Misra S, Yu L, Foldyna M and Roca i Cabarrocas P 2013 High efficiency and stable hydrogenated amorphous silicon radial junction solar cells built on VLS-grown silicon nanowires *Sol. Energy Mater. Sol. Cells* **118** 90–5

[18] Suematsu K, Shin Y, Hua Z, Yoshida K, Yuasa M, Kida T and Shimanoe K 2014 Nanoparticle

cluster gas sensor: Controlled clustering of SnO2 nanoparticles for highly sensitive toluene detection *ACS Appl. Mater. Interfaces* **6** 5319–26

[19] Leite E R, Giraldi T R, Pontes F M, Longo E, Beltrán A and Andrés J 2003 Crystal growth in colloidal tin oxide nanocrystals induced by coalescence at room temperature *Appl. Phys. Lett.* **83** 1566–8

[20] Girard H A, Perruchas S, Gesset C, Chaigneau M, Vieille L, Arnault J C, Bergonzo P, Boilot J P and Gacoin T 2009 Electrostatic Grafting of Diamond Nanoparticles: A Versatile Route to Nanocrystalline Diamond Thin Films *ACS Appl. Mater. Interfaces* **1** 2738–46

[21] Kim J, Dantelle G, Revaux A, Bérard M, Huignard A, Gacoin T and Boilot J-P 2010 Plasmon-Induced Modification of Fluorescent Thin Film Emission Nearby Gold Nanoparticle Monolayers *Langmuir* **26** 8842–9

[22] Sabat K C, Rajput P, Paramguru R K, Bhoi B and Mishra B K 2014 Reduction of Oxide Minerals by Hydrogen Plasma: An Overview *Plasma Chem. Plasma Process.* **34** 1–23

[23] Rasband, W.S., ImageJ, U. S. National Institutes of Health, Bethesda, Maryland, USA, https://imagej.nih.gov/ij/, 1997-2016.

[24] Gohin M, Allain E, Chemin N, Maurin I, Gacoin T and Boilot J P 2010 Sol-gel nanoparticulate mesoporous films with enhanced self-cleaning properties *J. Photochem. Photobiol. A Chem.* **216** 142–8

[25] Kosmulski M 2009 Compilation of PZC and IEP of sparingly soluble metal oxides and hydroxides from literature *Adv. Colloid Interface Sci.* **152** 14–25

[26] Zhan S, Li D, Liang S, Chen X and Li X 2013 A novel flexible room temperature ethanol gas sensor based on SnO_2 doped poly-diallyldimethylammonium chloride *Sensors (Switzerland)* **13** 4378–89

[27] Kim B-S, Lee J-C, Yoon H-S and Kim S-K 2011 Reduction of SnO_2 with Hydrogen *Mater. Trans.* **52** 1814–7

[28] Wallinga J, Arnoldbik W M, Vredenberg a M, Schropp R E I and Van Der Weg W F 1998

Reduction of Tin Oxide by Hydrogen Radicals *J. Phys. Chem. B* **102** 6219–24

[29] Tang J, Maurice J-L, Chen W, Misra S, Foldyna M, Johnson E V. and Roca i Cabarrocas P 2016 Plasma-Assisted Growth of Silicon Nanowires by Sn Catalyst: Step-by-Step Observation *Nanoscale Res. Lett.* **11** 455